

Diagenetic evolution of a fractured evaporite deposit (Vilobí Gypsum Unit, Miocene, NE Spain)

M. MORAGAS^{1,2}, C. MARTÍNEZ², V. BAQUÉS², E. PLAYÀ², A. TRAVÉ², G. ALÍAS² AND I. CANTARERO²

¹Group of Dynamics of the Lithosphere (GDL), Institute of Earth Sciences Jaume Almera, ICTJA-CSIC, Barcelona, Spain;

²Departament Geoquímica, Petrologia i Prospecció Geològica, Facultat de Geologia, Universitat de Barcelona (UB), Barcelona, Spain

ABSTRACT

The upper Burdigalian Vilobí Gypsum Unit, located in the Vallès Penedès half-graben (NE Spain), consists of a 60-m thick succession of laminated-to-banded secondary and primary gypsum affected by Neogene extension in the western part of Mediterranean Sea. This Tertiary extensional event is recorded in the evaporitic unit as six fracture sets (faults and joints), which can be linked with basin-scale deformation stages. All fractures are totally or partially infilled by four types of new gypsum precipitates showing a large variety of textures and microstructures. A structural and petrological study of the unit allows us to establish the following chronology of the fracture formation and infilling processes, from oldest to youngest: (i) S1 and S2 normal faults sets formation and precipitation of sigmoidal gypsum fibres; (ii) S3 joint set formation and growing of perpendicular fibres; (iii) S4 inverse fault development, infilled by oblique gypsum fibres and deformation of the previous fillings; and (iv) S5 and S6 joint formations and later dissolution processes, infilled by macrocrystalline gypsum cements. The fractures provided the pathway for fluid circulation in the Vilobí Unit. The oxygen, sulphur and strontium isotope compositions of the host rocks and the new precipitates in the fractures suggest clear convective recycling processes from the host-sulphates to the fracture infillings, recorded by a general enrichment trend to heavier S–O isotopes, from the oldest precipitates (sigmoidal fibres) to the youngest (macrocrystalline cements) and to the preservation of the strontium signals in the infillings.

Key words: calcium sulphate fluid flow, Evaporites, microstructures, strontium isotopes, sulphur–oxygen isotopes

Received 27 July 2012; accepted 14 January 2013

Corresponding author: Mar Moragas, Group of Dynamics of the Lithosphere (GDL), Institute of Earth Sciences Jaume Almera, ICTJA-CSIC, Lluís Solé i Sabarís s/n, 08028 Barcelona, Spain and Departament Geoquímica, Petrologia i Prospecció Geològica, Facultat de Geologia, Universitat de Barcelona (UB), Martí i Franquès s/n, 08028 Barcelona, Spain. Email: mmoragas@ictja.csic.es. Tel: +349 34095410, Fax: +349 34110012.

Geofluids (2013) 13, 180–193

INTRODUCTION

Evaporite rocks are usually considered as ductile rocks under tectonic stresses, as they tend to deform and flow without rupture, due to their general low density and viscosity. Evaporites expulse their pore waters in the first tens of metres when buried; thus, they become nonporous and noncompressible rocks under burial conditions (Casas & Lowenstein 1989; De la Cueva 1992; Warren 1999). Salt and sulphate rocks have low permeability, very low solubility in hydrocarbons and no or very little porosity. Such rocks frequently develop large scale halokinetic structures (pillows, diapirs) associated with large oil and gas accumulations. Furthermore, they also serve as décollement horizons in foreland fold and thrust belts (De Meer *et al.*

2000; and references therein). Gypsum and anhydrite rocks show a different mechanical behaviour than carbonates. Even under moderate stresses, anhydrite can develop structures generally observed in metamorphic rocks, such as microfolding, boudinage, foliation, stretching lineation, shear bands and recrystallization (Mosso 1973; Marcoux *et al.* 1987; Lugli 2001; Rouchy & Blanc-Valleron 2006; Torres *et al.* 2012). Anhydrite is believed to show a more rigid behaviour than gypsum; anhydrite fragments have been described as rigid objects that develop spectacular gypsum pressure shadows in décollement zones (Triassic evaporites) from the Southern Alps (Malavieille & Ritz 1989).

Despite the very ductile behaviour of gypsum and anhydrite rocks, the Vilobí Gypsum Unit shows several totally

or partially filled fracture sets, unrelated to folding or other ductile structures; thus, the unit has suffered brittle deformation, and fluids have flowed along the fracture planes. Fracture processes and fluid flow evolution in evaporites are poorly understood in the literature. As stated above, most of the references are dedicated to ductile deformation and microstructures. For example, Sadooni (1995) describes fractured sulphates, but he associates such brittle mechanisms to folding.

Most of the literature dealing with gypsum precipitates in fracture pays attention to the satin spar (fibrous) gypsum veins, as the origin of these infillings has been under great debate (Shearman *et al.* 1972; Machel 1985; Marcoux *et al.* 1987; Gustavson *et al.* 1994; El Tabakh *et al.* 1998; Philipp 2008). All these authors agree that fibrous fillings are cements in opened fracture planes and mainly assume that rehydration of anhydrite rocks and expulsion of CaSO_4 -rich fluids are the origin of the parental fluids. But in general, satin spar veins are horizontal and exclusively display fibrous gypsum; combination of several cements in fractures and/or gypsum cements in nonstrata-bound fractures have not been described in the literature, but they have been recognized in the studied evaporite unit.

The main objectives of this study are: (i) to determine the parental fluids of the fracture infillings and the evolution of the fluids during the different precipitation events, according to the whole diagenetic history of the unit; and (ii) to establish direct relationships between the local deformation stages and the regional deformation events, paying special attention to the fragile deformation structures.

GEOLOGICAL SETTING

The Vilobí Gypsum Unit is located in the Penedès half-graben, which is located in the Catalan Coastal Ranges, at the NE part of Iberian Peninsula (Fig. 1). The Catalan Coastal Ranges represent the continental northern margin of the Valencia Trough, which is a large NE-SW orientated basin developed as a result of the regional extensive Neogene event, which affected the western Mediterranean. The Valencia Trough is an oil-producing basin where accumulations are in Mesozoic and Neogene rocks; over a hundred wells have been drilled in the Valencia Trough since initial discovery in 1970. The most important fields are the Amposta and Casablanca oil exploitations (Clavell & Berastegui 1991; Varela *et al.* 2005; Playà *et al.* 2010; Rodríguez-Morillas *et al.* 2013).

The Catalan Coastal Ranges are mainly constituted by a NE-SW oriented horst and graben system developed during Neogene extension, resulting from the reactivation of previous compressive fractures developed during the regional Paleogene contraction (late Eocene-early Oligocene) (Roca 1994; Cabrera *et al.* 2004; Gaspar-Escribano *et al.* 2004). Part of the Valencia Trough and the present Cata-

lan Coastal Ranges were uplifted during this compressive event and during the late Oligocene-early Miocene, the compressional structures were overprinted by extensional faulting related to a regional rifting stage (giving rise to the NE-SW trending). That regional Neogene extension was characterized by two main stages: a syn-rift episode developed between late Oligocene and early Burdigalian, and a thermal subsidence stage from the latest Burdigalian to Quaternary. The thermal subsidence stage was not a continuous stage because minor steps can be differentiated (Bartrina *et al.* 1992; Roca & Guimerà 1992; Roca *et al.* 1999): (i) Quiescent stage with little tectonic activity stage (late Burdigalian-early Serravallian); (ii) brief reactivation stage (late Serravallian-Messinian) including minor strike-slip and compressive events, Serravallian and Messinian in age; and (iii) attenuation of extensional activity (Pliocene-present) (Bartrina *et al.* 1992; Roca 1994; Travé & Calvet 2001).

The thickness of the Neogene sediment filling the Penedès basin reaches up to 4000 m. As a consequence of the rifting stage, followed by thermal subsidence, several transgressive pulses in the upper Burdigalian to Langhian led to a partial flooding of the western part of the basin by sea water changing to nonmarine conditions, which have prevailed up to present (Cabrera 1981). The basin exhibits a heterogeneous sediment filled with continental clastics, marine deposits including reefs build-ups and sabkha-salina evaporite sediments.

METHODS

This structural study was carried out in the region where evaporites crops out. We collected approximately 80 fracture plane measurements, which were chronologically arranged according to their crosscutting relationships. Sixty-one samples of host gypsum rocks and fracture infillings (gypsum) were collected, and twenty standard thin sections were prepared. Petrological and microstructural studies were performed using optical and scanning electron microscope (ESEM QUANTA 200 with a X-ray microanalysis device-EDAX Genesi). Twenty-two powdered samples were analysed by X-ray diffraction for a mineralogical characterization in a Bragg-Brentano PANalytical X'Pert PRO MPD alpha-1 diffractometer.

All the powdered gypsum samples were first reacted with HCl 2 N before carrying out the geochemical analyses, to remove carbonate fraction and part of celestite content (Lucchesi & Whitney 1962; Playà & Rosell 2005).

The $\delta^{18}\text{O}_{\text{VSMOW}}$ and $\delta^{34}\text{S}_{\text{VCDT}}$ values of the sulphates, in, were analysed in fifty-one gypsum samples all converted to BaSO_4 . The respective CO and SO_2 gases produced from the sulphates were analysed on a continuous-flow elemental analyser Finnigan DELTA plus XP mass spectrometer, with TC/EA pyrolyser for oxygen and Finnigan MAT

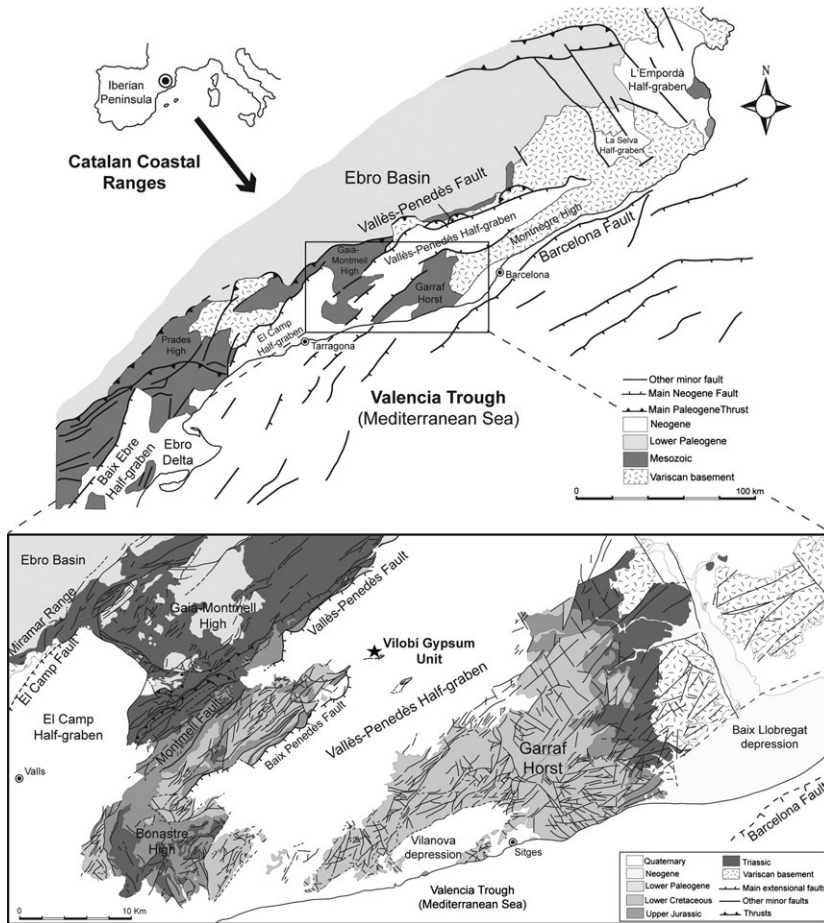


Fig. 1. Geological map of the Catalan Coastal Ranges and detail of the Penedès basin and studied area location (Vilobí del Penedès village, star in the figure) (Modified from Baqués *et al.* 2012b).

CHNS 1108 analyser for sulphur. The results are precise to 0.4 for $\delta^{34}\text{S}_{\text{VCDT}}$ and 0.5 for $\delta^{18}\text{O}_{\text{VSMOW}}$.

To determine $^{87}\text{Sr}/^{86}\text{Sr}$ ratios, ten samples of both host gypsum and fracture infillings were selected. The strontium and rubidium contents were first analysed to control possible contamination from celestite (Sr), while contribution of radiogenic ^{87}Sr coming from the ^{87}Rb decay (Rb). Samples were dissolved in 18 m Ω cm $^{-1}$ Milli-Q water; to avoid gypsum saturation in the final solution and to ensure a similar range of concentrations, a constant dilution ratio of 1:500 was maintained for all samples. The samples were then filtered through a 0.45- μm cellulose acetate and cellulose nitrate membrane filter to remove any quartz or other insoluble mineral particles. Sr contents were analysed in a ICP-OES with a Perkin Elmer, model Optima 3200RL, with wavelength of 421.552 nm, while Rb was charged in a Perkin Elmer ICP-MS, Elan 6000 model.

The ten powdered (and HCl 2N leached) samples were dissolved in Teflon PFA (Savillex[®]) vessels using HNO₃ 2N. The solutions were subsequently centrifuged to separate the fraction insoluble in acid. Chemical procedures for Sr extraction using the Sr-Spec resin of Eichrom. All the procedures were carried out in a clean room. The Sr fractions of the rock samples were measured for isotope

ratios by plasma ionization multicollector mass spectrometry (MC-ICP-MS) using a high-resolution Thermo Fisher Scientific Neptune instrument at the SGiker facility. The accuracy and reproducibility of the method were verified by periodic determinations under the same conditions using the NBS-987 strontium standard, averaging ($n = 4$) 0.710272 ± 0.000022 (2σ). The precision of the measurement is 0.0031% (2σ).

GYPSUM UNIT

The Vilobí Gypsum Unit is upper Burdigalian in age. The unit outcrops at the northwest of Vilobí village and is orientated NW-SE and dips 30° to the NE. This evaporite succession (60 m thick) is laying on nonmarine grey shales and limestones and is overlain by nonmarine red and grey shales and marine calcarenites (Langhian) (Ortí & Pueyo 1976; Bitzer 2004). These Tertiary deposits are separated by an erosional unconformity from the underlying Cretaceous carbonate rocks.

The unit consist of two subunits. The Lower Subunit is characterized by three different textural varieties that progressively evolve into the other with no defined boundaries, preserving the depositional lithofacies (laminated-to-

banded gypsum alternating with thin carbonate laminae) (Ortí & Pueyo 1976; Fig. 2). Several lutite levels, up to 20 cm thick, are interlayered in the evaporite unit. Part A of this subunit (Fig. 2) is up to 30 m thick and is texturally formed by micronodular–nodular fine-grained alabastrine (microcrystalline) gypsum. The following 20 m (part B) are formed by radial aggregates with diameters up to 10 cm. In the upper part (part C), the radial aggregates become larger enough (several tens of cm in length) allowing the identification of individual elongated and lenticular crystals crosscutting the bedding. Some enterolithic beds are intercalated throughout this gypsum interval. Under the microscope, all the textural varieties show anhydrite relics within the gypsum crystals (Fig. 2). Celestite is also a minor accessory mineral widely present in the whole unit.

The Upper Subunit (4 m thick) is characterized by laminated-to-banded gypsarenite and microselenite (grass-like) layers; crystals are sized up to 1 cm. Carbonate laminae and celestite are also present, and anhydrite is lacking. The contact with the secondary gypsum subunit is sharp.

FRACTURE SET ANALYSIS

Up to 6 fracture sets (faults and joints) have been identified and related to different deformation events (Fig. 3):

- (1) The first two fracture sets (S1 and S2) consist of coeval conjugate normal faults structures. S1 consists of NE-SW trending extensional faults dipping between 33 and 70° SE (mean of 50°). S2 is composed of a normal fault system trending NE-SW with a mean dip value of 50° NW (from 38 to 80°) (Fig. 3). Both sets of fractures are nonstrata-bound, showing scale spacing up to 10 m, lengths of up to 10 m and displacement in the order of cm–dm (Fig. 4). In most cases, the fracture porosity has been enlarged by dissolution along the

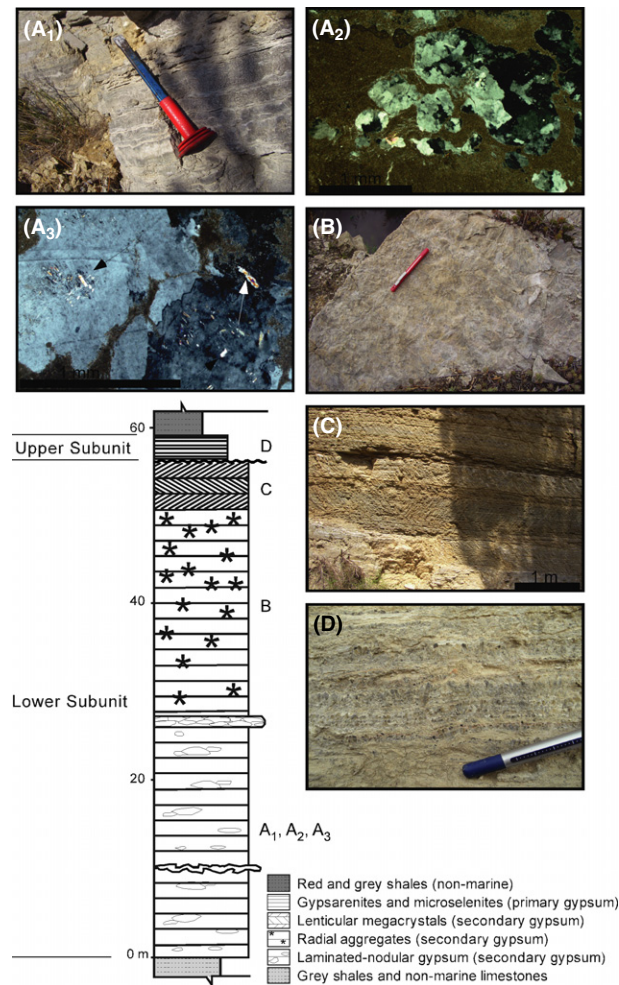


Fig. 2. Stratigraphic section of the Vilobí Gypsum Unit modified from Ortí & Pueyo (1976) of the different gypsum lithofacies. A, B, C and D mark the location of the samples in the section. A₁, A₂ and A₃, outcrop and microscope images of laminated-nodular gypsum lithofacies with anhydrite relics within secondary gypsum. B, radial aggregates, variety of secondary gypsum. C, lenticular gypsum crystals, variety of secondary gypsum. D, detail of gypsarenite lithofacies with interlayered microselenite levels.

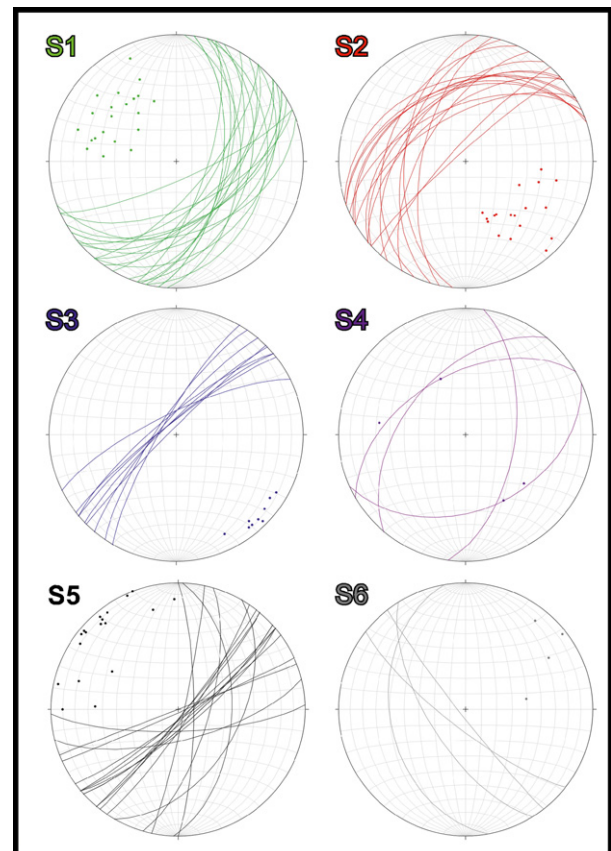


Fig. 3. Projections of fault and joints of the Vilobí Gypsum Unit outcrops defining six families. S1 and S2 normal faults are conjugate faults systems (SE and NW dipping, respectively). S3 joints are dipping towards the NW, whereas S4 thrust faults shows two main dip directions (SE and NW). S5 and S6 joints have SE and SW dip direction, respectively.

fracture plane, being more evident in the crosscutting areas. All fracture and cavern porosities (openings up to 10 cm) are totally filled by *sigmoidal fibrous* and/or *macrocrystalline gypsum cements*.

- (2) Set 3 (S3) is formed by NE-SW trending, subvertical, NW-dipping joints (Fig. 3) that crosscut S1 and S2, indicating a younger formation age. This set of fractures occurs very locally, in groups of three or four joints spaced cm to dm and up to 1 cm in width. These nonstrata-bound fractures have not been enlarged by dissolution, and they are totally filled by *perpendicular fibrous gypsum (satin spar)*.
- (3) Set 4 (S4) is made up of NE-SW trending thrust faults with both NW and SE dipping (Fig. 3). S4 fractures have a scattered presence in the Vilobí Gypsum Unit, corresponding only to 6% of the total recorded measurements. Fracture lengths range from 15 cm to 3 m and are randomly distributed throughout the unit (Fig. 4). These structures are totally filled by *oblique gypsum fibres*. The displacement of these structures is unknown.
- (4) S5 and S6 comprise two orthogonal sets of nonstrata-bound joints. S5, composed by SE-dipping joints with cm to dm spacing, is the most penetrative set, whereas

S6 (SW dipping) shows a scattered distribution throughout. The most penetrative surfaces (S5) are usually enlarged by dissolution, resulting in irregular boundaries. Openings by dissolution in some joints can reach 80 cm. Fracture porosity can be totally or partially filled by *macrocrystalline gypsum cements* or uncemented in the least penetrative planes.

GYP SUM VEINS AND CEMENTS

All fractures are filled by very pure gypsum crystals with 4 different microstructures and arrangements (Figs. 5 and 6): *Sigmoidal fibrous veins*, *perpendicular fibrous veins*, *oblique gypsum veins* and *macrocrystalline cements*. Macrocrystalline fillings are considered as cement, understanding ‘cements’ as new minerals precipitated in pore spaces (Tucker 1981; Boggs 2003). In the studied outcrops, the pore space is fracture and cavern porosity types (Choquette & Pray 1970; Tucker & Wright 1991; Moore 2001). The remainder gypsum precipitates in fractures are called gypsum veins, according to the vein definition as ‘mineral aggregates that precipitated from a fluid in dilatational sites’ (Bons *et al.* 2012).

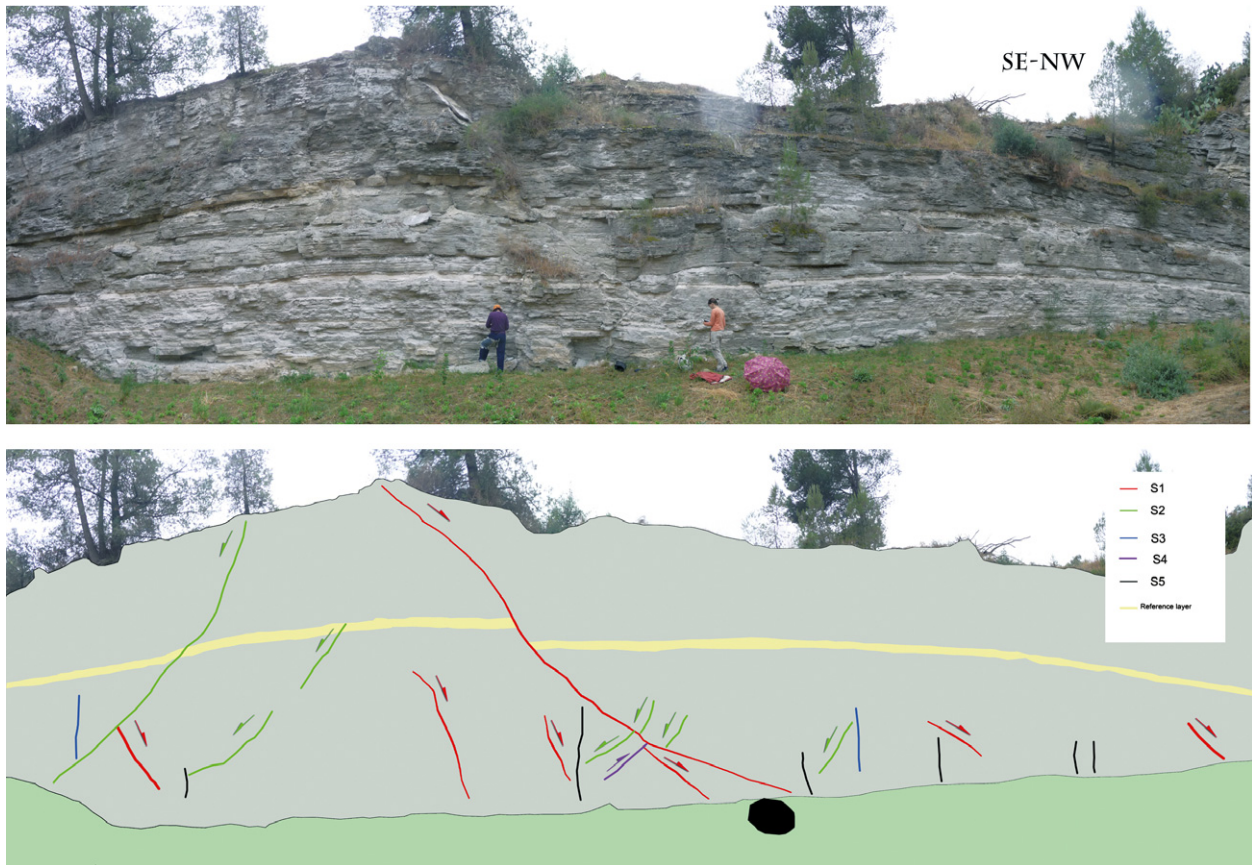


Fig. 4. Outcrop panorama of the Vilobí Gypsum Unit in which five of the six fracture sets are highlighted. (S1 red, S2 green, S3 violet, S4 blue, S5 black)

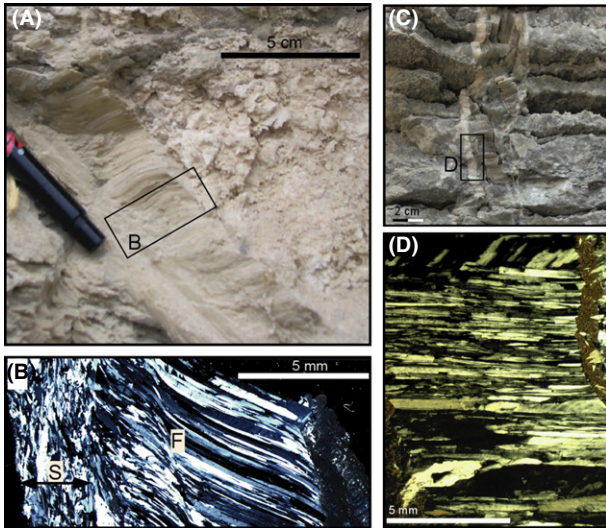


Fig. 5. Images of sigmoidal fibres (A & B) and perpendicular fibres (C & D). (A) Sigmoidal fibres linked with S1 and S2 faults. The rectangle indicates location of image B. (B) Photomicrography in cross-polarized light of sigmoidal fibrous gypsum (F) with two different stages of sigmoidal fibre development bounded by minor shear planes. Individual curved fibres show optical continuity. Small elongated crystals (S) are located near the wall rock. (C) Outcrop picture of S3 joint infilled by perpendicular fibrous gypsum (satin spar). (D) Photomicrography in cross-polarized light of fibres growing perpendicular to the joint walls with a thin median zone.

(1) *Sigmoidal fibrous veins*. These veins consist of fibres from 1 to 5 cm long filling S1 and S2 faults. Fibres show curved morphology and oblique orientation to the fault walls (Figs. 5A and B), with no visible median line in the veins. The fibrous crystals show constant thickness from fracture centre to fracture wall, precipitating in optical continuity and constant crystallographic orientation, and lack of wavy extinction and internal breakage (Fig. 5B). The fibres are commonly limited by microfractures and Riedel Y-shears within the fracture planes, indicating several growing fracturation events and a complex infilling history of the veins. Small elongated gypsum crystals are observed near the wall rock; these crystals, which are aligned parallel to the fault plane, are interpreted as broken sigmoidal fibres (Fig. 5B).

A few host gypsum fragments, up to 1 mm in size, are randomly embedded within the fibres, but always close to the fracture walls, indicating short displacement. Chips are subangular and isolated, uncommon in secondary micro- to macrocrystalline gypsum with carbonate matrix.

(2) *Perpendicular fibrous veins (satin spar)*. These veins are characterized by fibrous gypsum crystals from 250 μm to 0.5 cm in size, growing perpendicular to the S3 fracture walls (Figs. 5C and D). The crystal contacts are straight and display internal fracturation and wavy

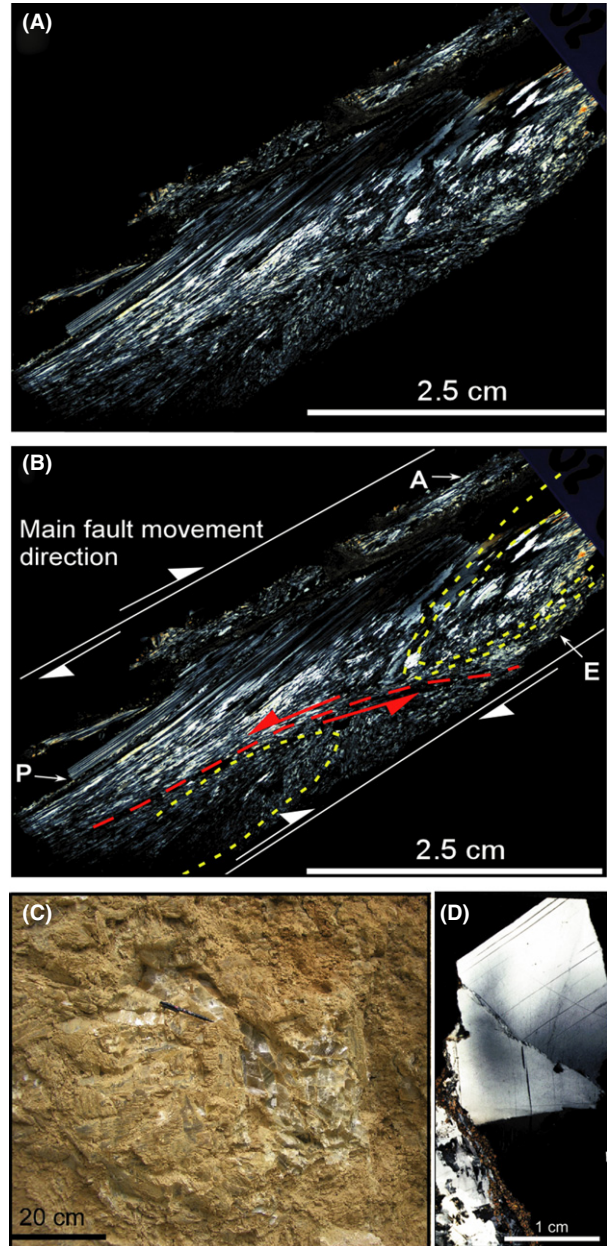


Fig. 6. (A) Thin section photomicrography in cross-polarized light from oblique fibrous gypsum (S4 infillings). (B) Interpreted thin section (A) showing the three different morphologies; (A) small crystals parallel to the fault wall, (P) stretched and elongated fibres with wavy extinction oblique to the fault wall, (E) anhedral crystals with wavy extinction. (C) Outcrop picture of macrocrystalline cements composed by gypsum crystals up to 20 cm in size. (D) Photomicrography in cross-polarized light of macrocrystalline gypsum showing wavy extinction; small euhedral gypsum crystals are between the macrocrystals.

extinction. The S3 veins sometimes display a median zone, parallel to the vein walls, dividing the gypsum fillings into two isopachous seams, equal in thickness and symmetrical (Fig. 5D). On a microscopic scale, the

parting is composed of microcrystalline secondary gypsum.

- (3) *Oblique gypsum veins*. These veins are mainly composed of fibres from <1 mm to 2 cm in length distributed parallel or slightly oblique to the walls of the S4 fracture planes. Several morphologies can be differentiated under microscope: short aligned crystals, large fibres and subeuhedral crystals. The aligned crystals (Fig. 6A) are short elongated gypsum crystals with wavy extinction close to the fracture walls, always in contact with the host gypsum. The large fibres are slightly oblique to the fault walls with wavy extinction, evolving gradually to subeuhedral elongated morphologies with irregular boundaries and wavy extinction.
- (4) *Macrocrystalline cement*. Euhedral (lenticular) to subeuhedral, but not twinned, gypsum, up to 20 cm, is found isotropically distributed mainly within S5 (and occasionally in S6) joints, displaying no changes in size from the wall to the centre of the cavities (Fig. 6B). Most of the joints have not been enlarged by dissolution and remain noncemented, but the most penetrative ones (S5) are usually enlarged by dissolution (creating cavern porosity) and are partially or totally cemented by large lenticular gypsum. The lenticules mainly precipitate along the c-axis parallel to the walls of the fractures, but are not developed completely where the fractures display little opening. These same macrocrystalline cements also infill some S1 and S2 fractures, accompanying the fibrous gypsum. In such cases, the macrocrystals mainly occur in the S1-S2 cross-points, in which fracture porosity has been enlarged by dissolution.

Macrocrystals show only local wavy extinction. Small euhedral gypsum crystals usually appear in the contact between the macrocrystals (suggesting crystal boundary recrystallization), and such recrystallized particles show oblique alignment (suggesting coeval movement during recrystallization) (Fig. 6C).

GEOCHEMISTRY

Sulphur and oxygen isotopes

Sulphur ($\delta^{34}\text{S}$) isotope analyses of the host gypsum rocks display a range of compositions from +20.9 to +22.3, in the basal secondary gypsum subunit, and between +17.8 and +21.8 in the upper gypsarenite-microselenite subunit. For oxygen ($\delta^{18}\text{O}$), secondary gypsum rocks show a range between +12.9 and +16.2, while the primary lithofacies are in a range from +15.6 to +18.6. These values are mostly within the range of the preexisting data (Agustí *et al.* 1990), but some samples of the primary subunit offer lighter sulphur compositions (Fig. 7, Table 1).

The oxygen and sulphur isotope compositions of gypsum infillings vary between +14.3 and +19.8, and from +21.8 to +25.1, respectively. Contrary to the host gypsum, which values plot in a dispersed area, the compositions of the infillings display a relatively good positive correlation. The $\delta^{34}\text{S}$ values clearly lighter than those of the host gypsum (Fig. 7, Table 1). Additionally, two groups of values are recorded within the infillings; the sigmoidal fibrous gypsum show lighter values, and the macrocrystalline cements display the heavier compositions (and also displaying a wider range of compositions).

$^{87}\text{Sr}/^{86}\text{Sr}$ analysis

Rb contents range from 32 to 285 ppb, while a wider range of Sr contents is defined (between 246 and 3498 ppm). The strontium isotope ratios are in a narrow range between 0.70863 and 0.70874. The most radiogenic values are in general displayed by the host gypsum rocks, while the sigmoidal fibrous gypsum offers the lowest one; the macrocrystalline cements show intermediate values (Fig. 8, Table 1).

DISCUSSION

Evaporite sedimentation and early diagenesis

The Vilobí Gypsum Unit succession is composed by two subunits (Fig. 2). According to Ortí & Pueyo (1976), the lower subunit is interpreted as precipitated in a coastal salina (laminated-to-banded gypsum lithofacies), which continuously evolved to a sabkha environment (enterolithic and nodular-micronodular anhydrite lithofacies). The growth of these anhydrite nodules is related to synsedimentary-early diagenetic processes in the sabkha environment. Nevertheless, this Lower Subunit was formed by secondary gypsum, after hydration of precursor anhydrite, evidenced by the gypsum textures (alabastrine and radial aggregates) and the presence of anhydrite relics. The mean isotopic signals for the lower gypsum are +21.5 and +14.3 for sulphur and oxygen, respectively, and the strontium isotope ratios are between 0.70863 and 0.70873 (Table 1). The S-O and Sr isotopic compositions of the Vilobí Gypsum suggest predominantly marine origin of the brines (Fig. 7). The Sr contents of these samples oscillate from 2240 to 3500 ppm, which is clearly due to celestite contamination.

The Upper Subunit in the Vilobí Gypsum is composed of a thin (few metres thick) interval of primary (depositional) gypsum, including laminated-to-banded microselenitic and gypsarenitic lithofacies, revealing a sedimentological change in the basin. Ortí & Pueyo (1976) interpreted this upper subunit as deposited in a coastal salina environment. Moreover, the sharp contact at its base can be interpreted as an

Table 1 $\delta^{34}\text{S}$, $\delta^{18}\text{O}$, $^{87}\text{Sr}/^{86}\text{Sr}$ and Sr and Rb content values of the host gypsum rocks and gypsum infillings.

Samples	Host gypsum	Cement type	$\delta^{18}\text{O}_{\text{VSMOW}}$ (‰)	$\delta^{34}\text{S}_{\text{VCDT}}$ (‰)	$^{87}\text{Sr}/^{86}\text{Sr}$	Sr content (ppm)	Rb content (ppb)
9226	Secondary gypsum*		12.4	21.2			
9227			12.3	20.4			
9230			12.8	21.5			
9235			13.5	21			
10203			17.5	21			
NA-4	Secondary gypsum		15.1	22.1			
NA-9			13.8	21.8			
NA-13			13.7	20.9			
ML-27			14.2	21.3			
VI-1			15.9	21.6	0.70863	3498	286
VI-3bc			14.6	22.1			
VI-5			13.9	21.9			
VI-11			12.9	21.8			
VI-32			16.2	21.5			
VI-34			15.5	21.7			
VI-65			14.9	22.3	0.70873	2240	67
VI-60	Primary gypsum		18.7	21.8	0.70871	1807	240
VI-62			15.6	17.8	0.70871	2667	214
GP-29			16.6	21.1			
GP-30			16.7	20.6			
VI-2		Sigmoidal fibres (S1-S2)	16.3	22.5	0.70863	246	97
VI-3aa			16.3	22.9			
VI-3ab			16.3	23.3			
VI-4			15.7	22			
VI-12aa			14.8	22.4			
VI-12ab			14.4	22.6			
VI-71a			14.3	21.5			
VI-100a			16.2	21.5			
VI-102a			15.7	22.6			
VI-3ba			16.6	23.5			
VI-36			19.4	21.8			
VI-39b			15.4	22.9			
VI-51b			14	22.3			
VI-53			14.8	22.2			
VI-70			14.6	23.3			
VI-72			14.9	22.6			
VI-102b			16.1	22.3			
VI-13		Perpendicular fibres (S3)	13.4	21.3			
VI-8 inf		Oblique cements (S4)	14.4	22			
VI-8 sup			13.7	22.6			
VI-103a			17.9	22.1			
VI-3bb		Macrocryalline cement (S1-S2)	17.4	23.4			
VI-7			14.9	22.6	0.70869	396	58
VI-9			17.9	24.2	0.70869	287	32
VI-33			19.4	23.8			
VI-38			17.9	24.3			
VI-39a			19.8	24.5			
VI-45			17.2	22.7			
VI-51a			16.8	22.9			
VI-52			18.3	24.3			
VI-64			16.2	22.5	0.70872	319	87
VI-71b			17.3	22.8			
VI-73			16	23.6			
VI-100b			17.7	21.4			
VI-103b			19.5	22.7			
VI-6		Macrocryalline cement (S5)	16.7	23.2	0.70869	374	82
VI-10			17.9	24.1			
VI-31			16.8	23.3			
VI-41			14.4	22.4			
VI-42			18.7	24.6			
VI-43			16	23.8			
VI-44			18.7	25.1	0.7087	382	63

*Data from Agustí *et al.* 1990.

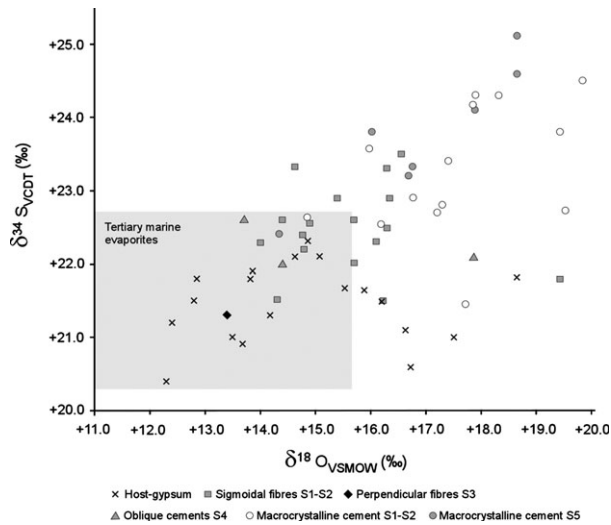


Fig. 7. $\delta^{34}\text{S}$ versus $\delta^{18}\text{O}$ cross-plot for both host gypsum rocks and gypsum infillings. Isotopic values for Tertiary marine evaporites comes from Utrilla *et al.* (1992).

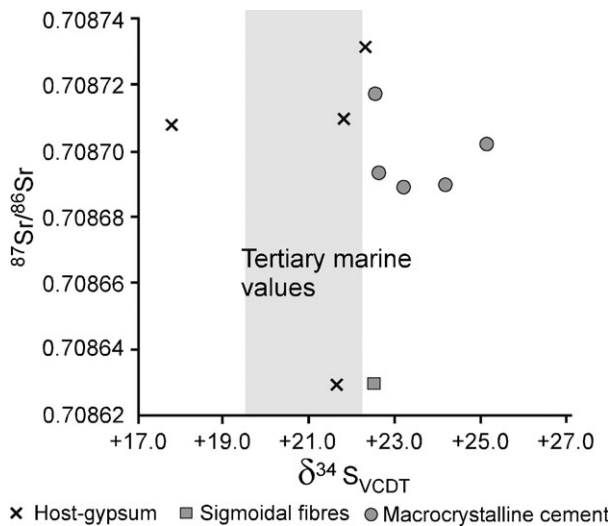


Fig. 8. $\delta^{34}\text{S}$ versus $^{87}\text{Sr}/^{86}\text{Sr}$ cross-plot for host gypsum, sigmoidal fibres and macrocrystalline cement samples. Sulphur isotope composition for Tertiary marine evaporites from Utrilla *et al.* (1992), whereas $^{87}\text{Sr}/^{86}\text{Sr}$ rates are taken from McArthur *et al.* (2001).

erosional dissolution surface and would have affected the large aggregates of secondary gypsum from the lower unit (Ortí 1990). Ortí & Pueyo (1976) suggested a complete diagenetic cycle (salina primary gypsum; sabkha anhydrite; rehydration to secondary gypsum), which would have occurred before the deposition of the upper interval of primary gypsum. The mean sulphur and oxygen isotopic values are +20.3‰ and +16.9‰, respectively, and the strontium ratio is 0.70871 (Table 1). Despite the prevalence of marine sulphate in the brines, a lowering of the sulphur isotope

compositions with respect to the lower subunit is detected, suggesting a nonmarine sulphate input in the basin at the top of the evaporite sequence evidenced by the presence of the red nonmarine (carophite-rich) clays that overlay the gypsum unit.

Deformation and infilling-cementation stages

The deformation history affecting the Vilobí Gypsum Unit can be divided in five events, all related to the major Neogene extensional event that occurred in the NW margin of the Mediterranean Sea (Fig. 9).

(1) *S1-S2 faults*: These are the main normal faults affecting the evaporite unit and the oldest fragile structure recorded. They are totally obliterated by sigmoidal gypsum fibres (stacking of several growing events limited by fractures), coexisting with macrocrystalline cements. Fibrous crystals growing oblique to the fracture walls and lacking wavy extinction and internal breakage suggest coeval movement of fractures during crystallization (El Tabakh *et al.* 1998). Fibrous morphologies are usually linked to a crystal growth rate occurring at the same rate as fracture opening (Machel 1985; El Tabakh *et al.* 1998). The studied gypsum fillings display a clear asymptotic trend of the fibres towards the walls supporting syntectonic precipitation. The small elongated crystals distributed parallel to the fracture wall with undulant extinction (Fig. 5), observed in some S1 and S2 fractures, could correspond to a fragmentation of previous crystals during this extensive event or later during the compressive event.

The main trend of the S1-S2 fractures and the direction of their movement are well correlated with the main basin structures (normal faults with NW-SE trend) produced during the Neogene rifting that affected the Vallès-Penedès basin (Banda & Santanach 1992; Bartrina *et al.* 1992). Taking into account that the evaporite unit was deposited during the upper Burdigalian (Cabrera 1981), these structures could not have developed during the syn-rift event (late Oligocene to early Burdigalian), but the evaporites probably fractured during the syn-rift to postrift transition (late Burdigalian to early Langhian), which is in accordance with a similar deformation event defined by (Baqués *et al.* 2012b).

(2) *S3 joints*: A gentle tectonic dilation was recorded by the subvertical S3 joints, in the latest early postrift stage, characterized by extension and a general decrease of tectonic activity. These small scale joints (S3) are filled by perpendicular fibrous crystals. Fibrous gypsum grows perpendicular to wall fractures symmetrically from a median zone. This vein type, generally called *satin spar* in the literature, commonly referred

Neogene extension stages	Ages	Vilobí Gypsum Unit			
		Fractures and dissolution processes	Cement type	Geochemistry	Fluid system
Late Post-Rift	Pliocene	?	?	$\delta^{18}\text{O} +14 - +21\text{‰}$ $\delta^{34}\text{S} +22 - +25.5\text{‰}$ $^{87}\text{Sr}/^{86}\text{Sr}$ 0.70869-0.70872	?
Minor compression	Messinian				
Late Post-Rift	Tortonian				
	Upper Serravalian	S5 and S6 joints and general dissolution processes	Macrocrystalline cements *	Recycling fluids	
Minor compression	Lower Serravalian - Upper Langhian	S4 thrust	Oblique gypsum cements	$\delta^{18}\text{O} +14.4\text{‰}$ $\delta^{34}\text{S} +22\text{‰}$	Seawater
Early Post-Rift	Upper Langhian	S3 joints	Perpendicular fibres cements	$\delta^{18}\text{O} +13 - +14\text{‰}$ $\delta^{34}\text{S} +21 - +22.5\text{‰}$	
	Lower Langhian	S1 and S2 faults	Sigmoidal fibres cements	$\delta^{18}\text{O} +12 - +19\text{‰}$ $\delta^{34}\text{S} +20.3 - +22\text{‰}$ $^{87}\text{Sr}/^{86}\text{Sr}$ 0.70863	
Syn-Rift	Upper Burdigalian	Vilobí Gypsum Unit precipitation and early diagenesis (anhydritization and rehydration)			

* Macrocrystalline cements were developed in several growing events from Upper Serravalian

Fig. 9. Relationship between fractures, infillings and fluid systems in the Vilobí Gypsum Unit linked to Neogene extensional stage developed in the Penedès half-graben.

to subhorizontal to slightly inclined planes (Machel 1985; Gustavson *et al.* 1994; El Tabakh *et al.* 1998; among others). In the S3 joints, however, they display a subvertical distribution.

- (3) *S4 faults*: These thrust faults show the same trend as the S1-S2 faults (Fig. 3) and developed taking advantage of previous normal faults (S1 and S2). Minor compressive events have been described in the Vallès-Penedès basin during both the upper Langhian-lower Serravalian and the Messinian (Bartrina *et al.* 1992; Roca 1994; Travé & Calvet 2001). Taking into account the crosscutting relationship between the six fracture sets defined in the Vilobí Gypsum Unit, the upper Langhian-lower Serravalian compressive event is the more reliable as the reactivation episode of the S1-S2 normal faults that promoted the formation of S4 thrust. This chronology is in agreement with the chronology established at basin scale by Baqués *et al.* (2012b).

At a microscope scale, compressive deformation is also observed in the fillings of the S4 fractures, which are mainly filled by oblique crystals, mainly composed of fibrous gypsum crystals orientated in a very low angle to the fracture walls and subeuhedral crystals with wavy extinction. These fibrous crystals developed synchronously to the evolution of S4 thrust. Their distribution (low angle to the wall vein) and morphology are linked to field stresses and low dilation rate linked to these structures, where fibrous growth direction is almost parallel to the vein offset direction (Bons & Monteneri 2005).

The subeuhedral crystals are interpreted as previously formed crystals, which were deformed during inverse fault activity, thus modifying their original distribution. The wavy extinction supports this interpretation, as is also indicated by a posterior deformation of the crystal (Hilgers and Urai 2002). However, it is impossible to determine whether the deformed crystals were

formed during the same tectonic event (early formed fibres) or whether they come from a previous stage (S1 and S2 fillings).

- (4) *S5-S6 joints*: After the minor compressive event, a general decrease in tectonic activity occurred in the studied area (Bartrina *et al.* 1992; Roca 1994), as recorded by S5 and S6 joints. Likewise, a general dissolution of the host rock in the fracture sectors is observed around outcrops, this dissolution process being more intense in intersection of several fractures and in the most penetrative S5 joints. In this context, large fracture opening allowed the precipitation of the macrocrystalline cements. Moreover, the crosscutting relationships between S5-S6 joints and S4 faults reveal that the joints developed after the lower Serravallian. The age of the dissolution is unknown, but could be tentatively attributed to the Messinian, taking into account the generalized sea level decrease in the Mediterranean area and the large dissolution processes occurring in the Vallès-Penedès basin due to the phreatic level fall (Baqués *et al.* 2012a).

Fluid flow evolution

Both the micro- to macrocrystalline gypsum of the Lower Subunit (Fig. 2) are diagenetic gypsum textures overprinted on the original laminated and nodular lithofacies, as indicated by the textural varieties of gypsum and the extensive presence of anhydrite relicts. Nevertheless, such laminated to nodular-enterolithic relict lithofacies suggest that the unit was precipitated in a marine sabkha-salina environment that evolved to salina deposits (gypsarenite and microselenite lithofacies) towards the top, probably coupled with the input of nonmarine fluids.

The $\delta^{34}\text{S}$ and $\delta^{18}\text{O}$ values of cements and vein fillings show a general isotopic enrichment trend, going from similar host rock isotopic values to heavier ones. The oldest fibrous gypsum, linked to the S1-S2 fractures (mean of +22.5 and +15.6 for sulphur and oxygen), shows the most similar isotopic values to those of the host gypsum rocks, which are close to Tertiary marine evaporite signatures. The macrocrystalline cements, which were precipitated in the latest deformation stages, show the most enriched isotopic values (mean of +24.6 and +18.3 for $\delta^{34}\text{S}$ and $\delta^{18}\text{O}$) (Fig. 7).

The observed tendency is easily explained by in situ chemical recycling, not by external basinal brine input. External brines could come into the area from the dissolution of Triassic evaporates, in which case the $\delta^{34}\text{S}$ would be more depleted than the obtained values. Fluids coming from interaction with Triassic evaporites in Spanish basins show $\delta^{34}\text{S}$ values between 14 and 16 according to Utrilla *et al.* (1992). The evolution of the latest cements to heavier values points to a continuous process of host dissolu-

tion and reprecipitation, taking into account that gypsum precipitation processes produce a sulphur fractionation of +1.65‰ (Thode & Monster 1965), whereas $\delta^{18}\text{O}$ enrichment is around +3.5‰ (Claypool *et al.* 1980). The higher oxygen enrichment, with respect to the sulphur enrichment, suggests successive chemical recycling processes from the host gypsum, the vein precipitates and finally the macrocrystalline cements.

The main source of the calcium sulphate ions is dissolution of the host Vilobí Gypsum Unit. The calcium sulphate-rich parental fluids flowed along the fractures, some of them enlarged by dissolution, recording changes in the isotopic signatures of the new gypsum precipitates. The source of Ca-SO_4 saturated fluids could have been first related to the early diagenetic anhydrite hydration. Such a process has been invoked in the literature as being responsible for some fibrous gypsum precipitates (Shearman *et al.* 1972). Nevertheless, the Vilobí Unit was tight, lithified and transformed to secondary gypsum (chips of host secondary gypsum are embedded within the veins fillings) when it started to fracture during the early postrift stage. This suggests that the anhydrite-gypsum transformation occurred before the fracture processes and that the Ca-SO_4 enriched fluids had already escaped. The absence of satin spar gypsum veins in the underlying and overlying lutite units supports this hypothesis. Initial sea water-related input in the first fibrous crystals cannot be ruled out, considering their marine-like sulphate isotopic signatures and the presence of Langhian marine facies close to the studied area, which coincide in age with the development of the S1-S2 faults and their coeval fibrous fillings (Baqués *et al.* 2012a). Sulphate chemical recycling and the onset of gypsum precipitation in fractures could have occurred in meteoric fluids and/or marine-related fluids.

The Sr contents in gypsum could come from direct incorporation from brine to crystals during crystallization or from external Sr inputs by means of celestite contamination or rubidium decay (Rosell *et al.* 1998; Playà & Rosell 2005). Rb and Sr contents were analysed to guarantee the Sr origin. Taking into account that no contamination by clay or celestite, evidenced by lower Sr content, occurs in the analysed strontium ratios of the infillings (from 200 to 400 ppm), nevertheless, slight differences exist between the fibrous crystals and the macrocrystalline cements (Fig. 8). For example, the $^{87}\text{Sr}/^{86}\text{Sr}$ values in the fibrous precipitates (0.70863) are less radiogenic than those of the macrocrystalline cements (values between 0.70869 and 0.70872). These isotopic signals fit with those of the marine Vilobí Gypsum Unit, thus reinforcing the chemical recycling of these gypsum host rocks.

Macrocrystalline gypsum grew in highly saturated calcium sulphate brines, promoting a reduced number of nuclei, slow crystallization rates and well-developed (euhedral) gypsum crystals. The cavern porosity (enlarged

fractures) is filled by randomly oriented lenticular crystals indicating no stratification of the brines and continuous flowing through the fractures. Because achievement of Ca-sulphate saturation in the brines is the key factor in the precipitation of these cements, this must be related to dissolution processes in gypsum rocks, not to evaporation processes. Slow fluid circulation rates along fractures and high fluid–host gypsum rock interaction are evidenced, promoting host gypsum dissolution. As the residence time of the brines is long suggesting a closed palaeohydrological system with a prolonged fluid–rock interactions with the host gypsum rocks. The more radiogenic strontium ratios in the macrocrystalline cements can be related to the presence of more radiogenic detrital components in the host gypsum rock, thus increasing the $^{87}\text{Sr}/^{86}\text{Sr}$ signatures of the cements.

CONCLUSIONS

The purpose of this study was to establish the parental fluids of the fracture infillings of the Vilobí Gypsum Unit and their evolution during the different precipitation events. Our results suggest that Vilobí Gypsum Unit was affected by a series of postrift deformation events of Neogene extension. As a result, six fracture sets formed at four different deformation stages linked to basin-scale events. In the early postrift (Langhian), S1 and S2 conjugated normal faults, and S3 joints were developed. Whereas S1 and S2 were totally filled by sigmoidal fibrous gypsum, which grew coeval to fault development, S3 was totally filled by perpendicular fibrous gypsum (satin spar gypsum veins).

Later, a minor compression occurred (lower Serravallian) originating the S4 inverse faults with the same orientation as S1 and S2 faults, most of which filled with oblique fibrous gypsum, which developed synchronously to the evolution of S4 fractures. Subeuhedral crystals, interpreted as previously formed crystals deformed during inverse fault activity, can be also related to these fracture infillings.

Finally, during the late postrift (upper Serravallian–Pliocene), the orthogonal system of the S5 and S6 joints were formed, followed by a general dissolution and a decrease in the tectonic activity in the basin. The most penetrative of these joints (S5) are totally or partially cemented by macrocrystalline gypsum, whereas the least penetrative (S6) remained uncemented.

Isotopic analysis provide compelling evidence for a closed (convective) hydrologic system associated with the formation of the fracture-filling cements. The $\delta^{34}\text{S}$ and $\delta^{18}\text{O}$ values of cements and vein fillings show a general isotopic enrichment trend, going from similar host rock isotopic values to heavier ones. The oldest fibrous gypsum, linked to the S1–S2 fractures, shows the most similar isotopic values to the values of the host gypsum rocks, which

are close to Tertiary marine evaporite signatures. The macrocrystalline cements, which were precipitated in the latest deformation stages, show the most enriched isotopic values. This trend reveals chemical recycling processes linked to fluid flow along the fractures dissolving the closest sulphates. Each successive infilling event resulted from recycling of the preexisting gypsum. Strontium isotopic signals of fracture gypsum infillings fit with those of the marine Vilobí Gypsum host rocks, thus reinforcing the chemical recycling of these gypsum host rocks.

ACKNOWLEDGEMENTS

The present work was supported by the Spanish Government Projects CGL2009-11096 and CGL2010-18260, and the *Grup Consolidat de Recerca Geologia Sedimentària* (Catalan Government) 2009SGR-1451. Strontium isotopic analyses were performed in the SGIker-Geocronología (Universidad del País Vasco), while the oxygen and sulphur isotope, Sr contents and SEM observations were carried out in the Centres Científics i Tecnològics (CCiT, Universitat de Barcelona, UB). The authors are indebted to Dr. Federico Ortí (UB) and Mr. Juan Morales (Universidad Complutense de Madrid) for their helpful comments, and Drs. Ihsan Al-Aasam (University of Windsor) and Paul D. Bons (University of Tubingen) are also thanked for their accurate revisions and valuable suggestions.

REFERENCES

- Agustí J, Cabrera L, Domènech R, Martinell J, Moyà-Solà S, Ortí F, De Porta J (1990) Neogene of Penedès area (Prelitoral catalan depression, NE Spain). In: *Iberian Neogene Basin: Field guidebook*, IXth Congress R.C.M.N.S., *Peleontologia i Evolució*, **2**, 187–208.
- Banda E, Santanach P (1992) The Valencia trough (western Mediterranean): an overview. *Tectonophysics*, **208**, 183–202.
- Baqués V, Travé A, Benedicto A, Cantarero I (2012a) Karstic systems development within the Baix Penedès Fault zone (onshore of the Valencia Trough, NW Mediterranean). *Geofluids*, This Volume.
- Baqués V, Travé A, Benedicto A, Cantarero I (2012b) The meteoric fluids circulation during the Miocene rifting of the Penedès Half-graben, NE Iberian Peninsula. In: *VIII Congreso Geológico de España*. Sociedad Geológica de España, Oviedo, Spain, Geo-Temas XIII.
- Bartrina MT, Cabrera L, Jurado MJ, Guimerà J, Roca E (1992) Evolution of the central Catalan margin of the Valencia trough (western Mediterranean). *Tectonophysics*, **203**, 219–47.
- Bitzer K (2004) Estimating paleogeographic, hydrological and climatic conditions in the upper Burdigalian Valle s-Penede basin (Catalunya, Spain). *Geologica Acta*, **2**, 321–31.
- Boggs S (2003) *Petrology of Sedimentary Rocks*, 1st edn, Blackburn Press, Cambridge, England.
- Bons PD, Montenari M (2005) The formation of antitaxial calcite veins with well-developed fibres, Oppaminda Creek, South Australia. *Journal of Structural Geology*, **27**, 231–48.

- Bons PD, Elburg MA, Gómez-Rivas E (2012) A review of the formation of tectonic veins and their microstructures. *Journal of Structural Geology*, **43**, 33–62.
- Cabrera L (1981) Influencia de la tectónica en la sedimentación continental de la cuenca del Vallés-Penedés (provincia de Barcelona, España) durante el Mioceno inferior. *Acta Geologica Hispánica*, **16**, 163–9.
- Cabrera L, Roca E, Garcés M, de Porta J (2004) Estratigrafía y evolución tectonosedimentaria oligocena superior - neógena del sector central del margen catalán. In: *Geología de España* (ed Vera JA), pp. 569–73. SGE-IGME, Madrid.
- Casas E, Lowenstein TK (1989) Diagenesis of saline pan halite: comparison of petrographic features of modern, Quaternary and Permian halites. *Journal of Sedimentary Petrology*, **59**, 724–39.
- Choquette PW, Pray LC (1970) Geologic nomenclature and classification of porosity in sedimentary carbonates. *American Association of Petroleum Geologists Bulletin*, **54**, 207–50.
- Clavell E, Berastegui X (1991) Petroleum geology of the Gulf of Valencia. *Generation, Accumulation, and Production of Europe's Hydrocarbons*, **1**, 355–368.
- Claypool GE, Holser WT, Kaplan IR, Sakai H, Zak I (1980) The age curves of sulfur and oxygen isotopes in marine sulfate and their mutual interpretation. *Chemical Geology*, **28**, 199–260.
- De la Cueva C (1992) Análisis del contenido en agua en formaciones salinas. Su aplicación al almacenamiento de residuos radioactivos. In: Unpublished, Universitat de Barcelona, PhD, 175.
- De Meer S, Spiers CJ, Peach CJ (2000) Kinetics of precipitation of gypsum and implications for pressure-solution creep. *Journal of the Geological Society*, **157**, 269–81.
- El Tabakh M, Schreiber BC, Warren JK (1998) Origin of fibrous gypsum in the Newark Rift Basin, Eastern North America. *Journal of Sedimentary Research*, **68**, 88–9.
- Gaspar-Escribano JM, García-Castellanos D, Roca E, Cloetingh E (2004) Cenozoic vertical motions of the Catalan Coastal Ranges (NE Spain): The role of tectonics, isostasy, and surface transport. *Tectonics*, **23**, 1–18.
- Gustavson TC, Hovorka SD, Dutton AR (1994) Origin of satin spar veins in evaporite basins. *Journal of Sedimentary Research A: Sedimentary Petrology and Processes*, **64**(A), 88–94.
- Hilgers C, Urai JL (2002) Microstructural observations on natural syntectonic fibrous veins: implications for the growth process. *Tectonophysics*, **352**, 257–74.
- Lucchesi BJ, Whitney ED (1962) Solubility of strontium sulphate in water and aqueous solutions of Hydrogen chloride, Sodium chloride, Sulphuric acid and Sodium sulphate by the radiotracer method. *Journal of applied chemistry*, **12**, 277–9.
- Lugli S (2001) Timing of post-depositional events in the Burano Formation of the Secchia valley (Upper Triassic, Northern Apennines), clues from gypsum-anhydrite transitions and carbonate metasomatism. *Sedimentary Geology*, **140**, 107–22.
- Machel HG (1985) Fibrous gypsum and fibrous anhydrite in veins. *Sedimentology*, **32**, 443–54.
- Malavieille J, Ritz JF (1989) Mylonitic deformation of evaporites in décollements: examples from the Southern Alps, France. *Journal of Structural Geology*, **11**, 583–90.
- Marcoux J, Brun JP, Burg JP, Ricou LE (1987) Shear structures in anhydrite at the base of thrust sheets (Antalya, Southern Turkey). *Journal of Structural Geology*, **9**, 555–61.
- McArthur JM, Howarth RJ, Bailey TR (2001) Strontium Isotope Stratigraphy: LOWESS Version 3: Best Fit to the Marine Sr-Isotope Curve for 0–509 Ma and Accompanying Look-up Table for Deriving Numerical Age. *The Journal of Geology*, **109**, 155–70.
- Moore CH (2001) *Carbonate Reservoirs: Porosity Evolution and Diagenesis in a Sequence Stratigraphic Framework*, p. 460. Elsevier Science Limited, Amsterdam.
- Mossop GD (1973) Anhydrite-Carbonate cycles of the Ordovician Baumann Fiord Formation, Ellesmere Island, Arctic Canada: A geological history. In: London, UK, Imperial College, Ph. D thesis.
- Ortí F (1990) Yesos de Vilobí (Mioceno). In: *Formaciones evaporíticas de la Cuenca del Ebro y cadenas periféricas, y de la zona de Levante* (eds Ortí F, Salvany JM), pp. 161–4, ENRESA, Departament de Geoquímica Petrologia i Prospecció Geològica, Universidad de Barcelona, Barcelona.
- Ortí F, Pueyo JJ (1976) Yeso primario y secundario del depósito de Vilobí (Provincia de Barcelona, España). *Instituto de Investigaciones Geológicas Universidad de Barcelona*, **31**, 5–34.
- Philipp SL (2008) Geometry and formation of gypsum veins in mudstones at Watchet, Somerset, SW England. *Geological Magazine*, **145**, 831–44.
- Playà E, Rosell L (2005) The celestite problem in gypsum Sr geochemistry: an evaluation of purifying methods of gypsiferous samples. *Chemical Geology*, **221**, 102–16.
- Playà E, Travé A, Caja MA, Salas R, Martín-Martín JD (2010) Diagenesis of the Amposta offshore oil reservoir (Amposta Marino C2 well, Lower Cretaceous, Valencia Trough, Spain). *Geofluids*, **10**, 314–33.
- Roca E (1994) Geodynamic evolution of the Catalan-Balearic Basin and neighbouring areas from Mesozoic to Recent (La evolución geodinámica de la Cuenca Catalano-Balear y áreas adyacentes desde el Mesozoico hasta la actualidad). *Acta Geologica Hispanica*, **29**, 3–25.
- Roca E, Guimerà J (1992) The neogene structure of the eastern Iberian margin: structural constraints on the crustal evolution of the Valencia trough (Western Mediterranean). In: *Geology and Geophysics of the Valencia Trough, Western Mediterranean* (eds Banda E, Santanach P), Tectonophysics, **203**, 1–4, 203–18.
- Roca E, Sans M, Cabrera L, Marzo M (1999) Oligocene to Middle Miocene evolution of the central Catalan margin (northwestern Mediterranean). *Tectonophysics*, **315**, 209–29.
- Rodríguez-Morillas N, Playà E, Travé A, Martín-Martín JD, Guerrero A (2013) Diagenetic processes in a partially dolomitized carbonate reservoir: Casablanca oil field, Mediterranean Sea, offshore Spain. *Geologica Acta*, **11**, in press.
- Rosell L, Ortí F, Kasprzyk A, Playà E, Peryt TM (1998) Strontium geochemistry of Miocene primary gypsum: Messinian of Southeastern Spain and Sicily and Badenian of Poland. *Journal of Sedimentary Research*, **68**, 63–79.
- Rouchy JM, Blanc-Valleron MM (2006) *Les évaporites: Matériaux singuliers, milieux extrêmes*. Paris.
- Sadooni FN (1995) Diagenetic features of some subsurface Tertiary-Cretaceous evaporites from northern Iraq. *Carbonates and Evaporites*, **10**, 45–53.
- Shearman DJ, Mossop G, Dunsmore H, Martin H (1972) Origin of Gypsum veins by hydraulic fracture. *Transactions of the Institute of Mining and Metallurgy. Section B Applied Earth Sciences*, **81**, 149–55.
- Thode HG, Monster J (1965) Sulfur-isotope geochemistry of petroleum, evaporites and ancient seas. *Memoirs American Association of Petroleum Geologists*, **4**, 367–77.
- Torres G, Playà E, Alías G, Correa A, Chong G, Pueyo JJ (2012) Transformaciones texturales y minerales de evaporitas en las facies de los esquistos verdes. Distrito minero Teresa del Colmo (N de Chile). In: *VIII Congreso Geológico de España*. Sociedad Geológica de España, Oviedo, Spain, Geo-Temas XIII.

- Travé A, Calvet F (2001) Syn-rift geofluids in fractures related to the early-middle Miocene evolution of the Vallès-Penedès half-graben (NE Spain). *Tectonophysics*, **336**, 101–20.
- Tucker ME (1981) *Sedimentary Petrology: An Introduction*, Blackwell Scientific Publications, Oxford.
- Tucker ME, Wright VP (1991) *Carbonate Sedimentology*, John Wiley & Sons, Oxford.
- Utrilla R, Pierre C, Orti F, Pueyo JJ (1992) Oxygen and sulphur isotope compositions as indicators of the origin of Mesozoic and Cenozoic evaporites from Spain. *Chemical Geology*, **102**, 229–44.
- Varela J, Vicente-Bravo JC, Navarro J, Esteban M, Martínez del Olmo W (2005) The oil fields in the Spanish Mediterranean Sea. In: *Asociación de Geólogos y Geofísicos Españoles del Petróleo (AGGEP)* (ed Martínez del Olmo W), pp. 121–30. Museo de Ciencias Naturales, Madrid, XXV Aniversario.
- Warren JK (1999) *Evaporites: Their Evolution and Economics*. Blackwell Science, Oxford.

GEOFLUIDS

Volume 13, Number 2, May 2013

ISSN 1468-8115

CONTENTS

- 99 **EDITORIAL: 2012 Paris Geofluids VII Conference Summary & Thematic Issue**
Rudy Swennen, Francois Roure, Jacques Pironon, Fadi H. Nader and Mark Person
- 101 **Synchrotron XRF and XANES investigation of uranium speciation and element distribution in fluid inclusions from unconformity-related uranium deposits**
A. Richard, J. Cauzid, M. Cathelineau, M.-C. Boiron, J. Mercadier and M. Cuney
- 112 **Age and genesis of the White Pine stratiform copper mineralization, northern Michigan, USA, from paleomagnetism**
D.T.A. Symons, K. Kawasaki and J.F. Diehl
- 127 **Modelling fault reactivation and fluid flow around a fault restraining step-over structure in the Laverton gold region, Yilgarn Craton, Western Australia**
Y. Zhang, P.M. Schaub, H.A. Sheldon, T. Poulet and A. Karrech
- 140 **Fluid channeling along thrust zones: the Lagonegro case history, southern Apennines, Italy**
T. Gabellone, M. Gasparri, A. Iannace, C. Invernizzi, S. Mazzoli and M. D'Antonio
- 159 **Diagenesis versus hydrothermalism and fluid-rock interaction within the Tuscan Nappe of the Monte Amiata CO₂-rich geothermal area (Italy)**
M. Gasparri, G. Ruggieri and A. Brogi
- 180 **Diagenetic evolution of a fractured evaporite deposit (Vilobí Gypsum Unit, Miocene, NE Spain)**
M. Moragas, C. Martínez, V. Baqués, E. Playà, A. Travé, G. Alías and I. Cantarero
- 194 **Geochemical simulations to assess the fluorine origin in Sierra de Gador groundwater (SE Spain)**
L. Daniele, M. Corbella, A. Vallejos, M. Díaz-Puga and A. Pulido-Bosch
- 204 **Quantification of diagenesis impact on the reservoir properties of the Jurassic Arab D and C members (Offshore, U.A.E.)**
F.H. Nader, E. De Boever, M. Gasparri, M. Liberati, C. Dumont, A. Ceriani, S. Morad, O. Lerat and B. Doligez
- 221 **Dedolomitization and reservoir quality: insights from reactive transport modelling**
L.-C. Escorcia, E. Gomez-Rivas, L. Daniele and M. Corbella
- 232 **Reflux dolomitization of the Upper Permian Changxing Formation and the Lower Triassic Feixianguan Formation, NE Sichuan Basin, China**
L. Jiang, C.F. Cai, R.H. Worden, K.-K. Li and L. Xiang
- 246 **Petroleum system evolution in the inverted Lower Saxony Basin, northwest Germany: a 3D basin modeling study**
B. Bruns, R. Di Primio, U. Berner and R. Littke

WILEY
Blackwell

Geofluids is abstracted/indexed in *Chemical Abstracts*

This journal is available online at Wiley Online Library.
Visit onlinelibrary.wiley.com to search the articles and register for table of contents and e-mail alerts.